Physics of Atomic Nuclei, Vol. 63, No. 5, 2000, pp. 859–869. From Yadernaya Fizika, Vol. 63, No. 5, 2000, pp. 929–939.

ELEMENTARY PARTICLES AND FIELDS
Theory

Can HERA Data Improve the LEP Constraints on the *WWV* Vertex?*

A. A. Likhoded and A. I. Onishchenko**, 1)**

Budker Institute of Nuclear Physics (Protvino Branch), Siberian Division, Russian Academy of Sciences, Protvino, Moscow oblast, 142284 Russia

Received May 19, 1999; in final form, August 17, 1999

Abstract—The combined results from $ep \longrightarrow \nu WX$, $ep \longrightarrow eWX$, and $ep \longrightarrow \nu\gamma X$ processes at HERA are used to constrain anomalous three-boson couplings. The effective model for anomalous couplings where there is no light Higgs boson and where interactions responsible for the breakdown of electroweak symmetry are strongly coupled is considered. Bounds on the couplings L_{9L} and L_{9R}, which parametrize contributions from the anomalous $WW\gamma$ (WWZ) vertices, attainable from an analysis of the distributions for the processes in question are presented. The results are compared with the bounds resulting from the LEP I and LEP II data. It is shown that the bounds coming from HERA significantly reduce the parameter region allowed by the analysis of the LEP I and LEP II data. © *2000 MAIK "Nauka/Interperiodica".*

1. INTRODUCTION

One of the main goals of the operating LEP II and of future next linear colliders is to measure the $WW\gamma$ and WWZ couplings. In the Standard Model (SM), these couplings are strictly fixed by the structure of $SU(2) \times U(1)$ symmetry, and any deviation of the couplings from the values predicted by the SM will definitively indicate the presence of new physics. It is convenient to describe the phenomenology of models with anomalous couplings in terms of the low-energy effective Lagrangians. Within this approach, effects of new physics manifest themselves as higher dimension operators modifying the couplings of observed particles, including anomalous boson couplings. This approach has a number of practical consequences in limiting the number of anomalous couplings to be studied.

In this article, we consider a class of models where interactions responsible for electroweak-symmetry breaking are strongly coupled and where there are no new particles light enough to be produced at energies below 500 GeV–1 TeV and study the effect of the lowest dimension operators that lead to anomalous contribution of the $WW\gamma(Z)$ vertex at HERA energies. Deviations from the boson self-couplings predicted by the minimal SM were studied extensively in the literature; in particular, they were discussed in the context of the HERA collider [1–6]. The main processes to probe the anomalous couplings at the HERA collider are $ep \longrightarrow \nu\gamma X$, $ep \longrightarrow eWX$, and $ep \longrightarrow \nu WX$, where X is a hadronic state. The first two processes reveal sizable cross sections, which allow one to reconstruct final states and to analyze relevant distributions for the processes. In turn, the cross section for the process $ep \longrightarrow \nu WX$ is too small, so that only isolated events can be observed at the present HERA luminosity. For this reason, the chance to probe the anomalous couplings via this process was usually neglected. We will show later, however, that this process is highly sensitive to anomalous contributions, permitting the inclusion of data on this process in the analysis as well.

There are two main distinctions between the present study and those that can be found in the literature. First, we apply the effective Lagrangian formalism allowing us to parametrize the anomalous gauge-boson interactions and to correlate them with the symmetry-breaking sector. Second, we perform a global analysis of all three processes, $ep \longrightarrow \nu\gamma X$ (eWX, νWX). Here, we pay special attention to the fact that the process $ep \longrightarrow \nu WX$, in spite of the small cross section, reveals a high sensitivity to anomalous terms and leads to bounds competitive with those from the process $ep \longrightarrow eWX$ and more stringent than those coming from the data on radiative charged-current scattering.

This article is organized as follows. In Section 2, we briefly summarize the effective Lagrangian formalism used to describe anomalous couplings. In Section 3, we present the results of our calculations for the HERA processes. In Section 4, we present bounds on the anomalous couplings parametrizing the triple boson vertex and compare these bounds with those coming from LEP I and LEP II data. Finally, we summarize our results.

* This article was submitted by the authors in English.

** e-mail: likhoded@mx.ihep.su
*** e-mail: onishchenko@heron.itep.ru
1) Institute for Theoretical and Experimental Physics, Bol'shaya Cheremushkinskaya ul. 25, Moscow, 117259 Russia.

2. FORMALISM FOR ANOMALOUS COUPLINGS

Introducing anomalous boson interactions, we want to describe the case where, for the electroweak-symmetry-breaking sector, there is no light Higgs boson and where the low-energy particle content is essentially the same as that in the minimal SM, provided that Higgs boson is taken to be very heavy. This model can be written as the usual Standard Model, but the scalar sector must then be replaced by the effective Lagrangian [7]

$$\mathcal{L}^{(2)} = \frac{v^2}{4}\mathrm{tr}(D^\mu\Sigma^\dagger D_\mu\Sigma).$$

Here, the matrix $\Sigma \equiv \exp(i\boldsymbol{\omega}\cdot\boldsymbol{\tau}/v)$ contains the would-be Goldstone bosons ω_i that give the gauge bosons their mass via the Higgs mechanism, the $SU(2)_L \times U(1)_Y$ covariant derivative is given by

$$D_\mu\Sigma = \partial_\mu\Sigma + \frac{i}{2}gW_\mu^i\tau^i\Sigma - \frac{i}{2}g'B_\mu\Sigma\tau_3,$$

and $v \approx 246$ GeV. This case was considered at length in the literature [7, 8], and we used it previously for processes incorporating triple [9] and quartic boson interactions [10]. In this model, anomalous gauge-boson couplings correspond to the contributions from higher dimension operators that are invariant under the $SU(2)_L \times U(1)_Y$ gauge group. The next-to-leading-order (NLO) effective Lagrangian that arises in the context of this model and the contributions of this Lagrangian to the anomalous couplings were discussed in the literature [7, 8].

It became common to write the most general C- and P-invariant VW^+W^- vertex (where $V = Z, \gamma$) in the form [11]

$$\begin{aligned}\mathcal{L}_{WWV} = &-ie\frac{c_W}{s_W}g_1^Z(W^\dagger_{\mu\nu}W^\mu - W_{\mu\nu}W^{\mu\dagger})Z^\nu \\ &- ieg_1^\gamma(W^\dagger_{\mu\nu}W^\mu - W_{\mu\nu}W^{\mu\dagger})A^\nu \\ &- ie\frac{c_W}{s_W}\kappa_Z W^\dagger_\mu W_\nu Z^{\mu\nu} - ie\kappa_\gamma W^\dagger_\mu W_\nu A^{\mu\nu},\end{aligned} \quad (1)$$

where s_W and c_W are the sine and the cosine of the Weinberg angle.

At the tree level and in the unitary gauge, the anomalous terms contribute to the processes under consideration only through the three-gauge-boson vertex WWV. Within the effective Lagrangian approach and under the assumption that whatever breaks electroweak symmetry has at least an approximate custodial symmetry, there are only three operators in the C- and P-preserving NLO effective Lagrangian that are relevant to the gauge sector:

$$\begin{aligned}\mathcal{L}^{(4)} = \frac{v^2}{\Lambda^2}\{&-gL_{9L}\mathrm{tr}(W^{\mu\nu}D_\mu\Sigma D_\nu\Sigma^\dagger) \\ &- ig'L_{9R}\mathrm{tr}(B^{\mu\nu}D_\mu\Sigma^\dagger D_\nu\Sigma) \\ &+ gg'L_{10}\mathrm{tr}(\Sigma B^{\mu\nu}\Sigma^\dagger W_{\mu\nu})\}.\end{aligned} \quad (2)$$

However, it was shown in [12] that the coupling L_{10}, being proportional to the parameter ϵ_3 measured at LEP I, is tightly constrained, $-1.1 \le L_{10}(M_Z) \le 1.5$; therefore, we will not consider the evolution of this coupling.[2)]

For the case of a strongly interacting symmetry-breaking sector, the approach of the effective Lagrangian allows one to relate the four couplings in (1) to those in (2):

$$\begin{aligned}g_1^Z &= 1 + \frac{e^2}{c_W^2}\left(\frac{1}{2s_W^2}L_{9L} + \frac{1}{(c_W^2 - s_W^2)}L_{10}\right)\frac{v^2}{\Lambda^2} + \ldots, \\ g_1^\gamma &= 1 + \ldots, \\ \kappa_Z &= 1 + e^2\left(\frac{1}{2s_W^2c_W^2}(L_{9L}c_W^2 - L_{9R}s_W^2)\right. \\ &\quad \left. + \frac{2}{(c_W^2 - s_W^2)}L_{10}\right)\frac{v^2}{\Lambda^2} + \ldots, \\ \kappa_\gamma &= 1 + \frac{e^2}{s_W^2}\left(\frac{L_{9L} + L_{9R}}{2} - L_{10}\right)\frac{v^2}{\Lambda^2} + \ldots.\end{aligned} \quad (3)$$

In (3), the leading contribution to each anomalous coupling is presented, while the ellipses stand for contributions that arise in a higher order of $1/\Lambda^4$ or in the $1/\Lambda^2$ order with custodial $SU(2)$-symmetry breaking. It should be noted here that, in contrast to the anomalous couplings from [11], we do not have terms that correspond to the usual couplings λ_Z and λ_γ, because, within the model discussed, they only occur in higher orders in $1/\Lambda^2$.

In this paper, we will consider the processes $ep \longrightarrow \nu\gamma X$ (eWX, νWX) at the tree level and use the unitary gauge. In Figs. 1–3, one can see that new physics contributes to these processes via anomalous triple boson vertices, so that (adopting that L_{10} is severely constrained by LEP I data and that boson–fermion vertices remain unchanged) we are left with the set of anomalous couplings $g_1^{Z(\gamma)}$ and $\kappa_{Z(\gamma)}$ [in terms of (1)], or with the set of L_{9L} and L_{9R} [in terms of (2)].

3. PROCESSES WITH ANOMALOUS $WW\gamma(Z)$ COUPLINGS

In this section, we would like to discuss the possible manifestations of anomalous $WW\gamma(Z)$ couplings in the processes $ep \longrightarrow \nu\gamma X$ (eWX, νWX) at the HERA ep collider, where $E_e = 30$ GeV and $E_p = 820$ GeV, which corresponds to $\sqrt{s} = 314$ GeV. We adopt the integrated luminosity of 1000 pb^{-1}, which corresponds at least to five years of machine operation. We use a Monte Carlo

[2)]Within the model discussed, the anomalous couplings also affect the $Wf\nu$ and $Zf\bar{f}$ vertices through renormalization, but they do this only through the parameter L_{10} [12], and this contribution is neglected.

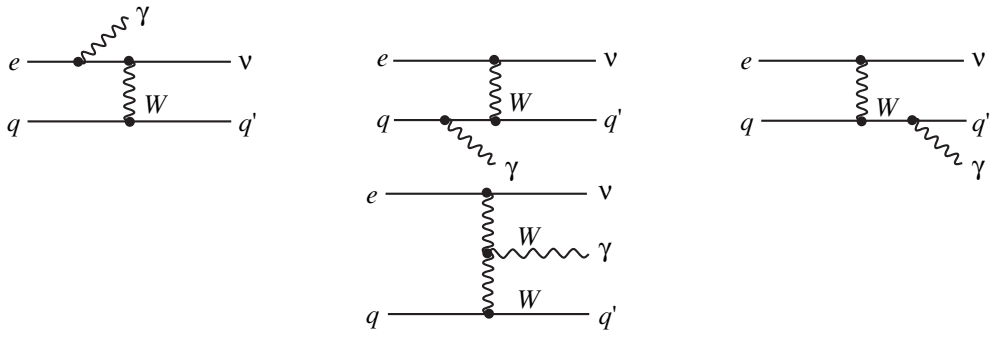

Fig. 1. Feynman diagrams for the process $ep \longrightarrow \nu\gamma X$.

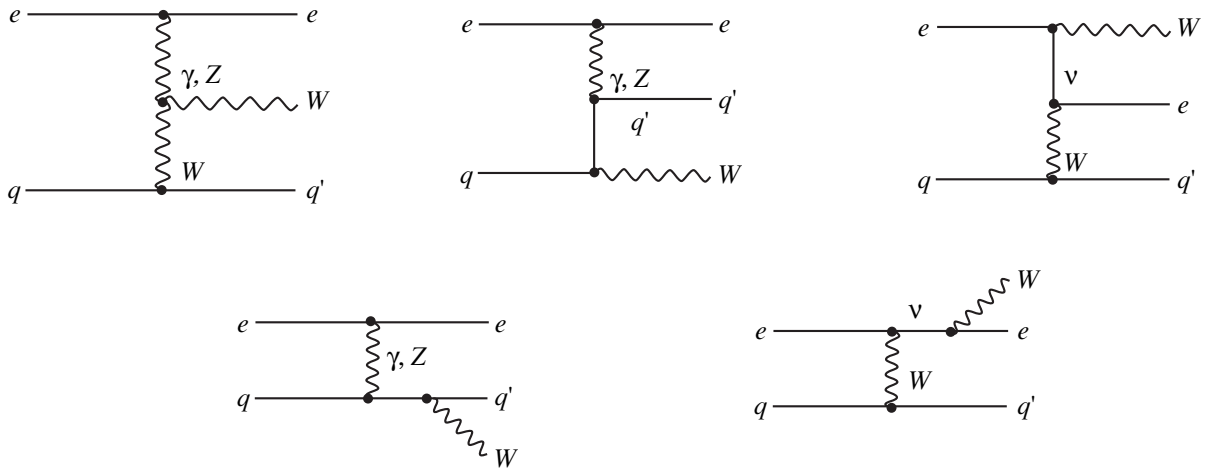

Fig. 2. Feynman diagrams for the process $ep \longrightarrow eWX$.

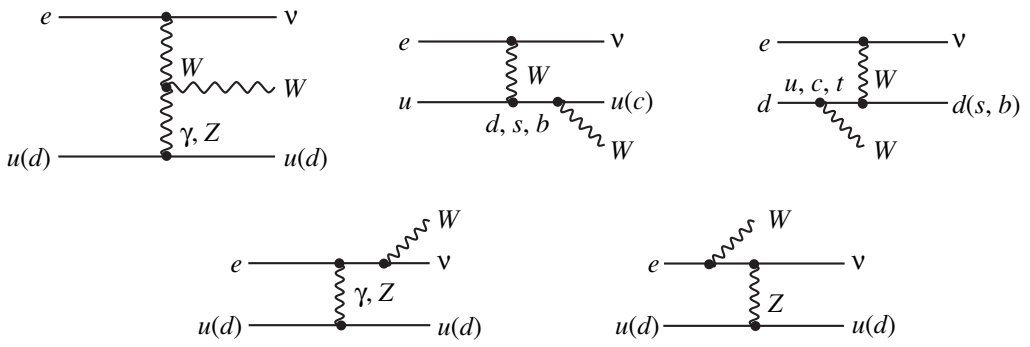

Fig. 3. Feynman diagrams for the process $ep \longrightarrow \nu WX$.

generator to simulate signal events and CTEQ4 parametrization [13] for the proton structure function. Standard sets of cuts on p_T^{jet}, p_T^{γ}, and p_T^{e}, as well as on the corresponding rapidities, were applied to satisfy the detector geometry and to reproduce the reconstruction efficiency. Uncertainties in the photon and jet energy measurements were taken into account by the Gaussian smearing of the 4-momenta. For our numerical study, we also use the following input parameter values:

$$M_W = 80.43 \text{ GeV}, \quad M_Z = 91.187 \text{ GeV},$$
$$\alpha = 1/128.8;$$

the values for CKM matrix elements were taken from the PDG review [14].

3.1. Process $ep \longrightarrow \nu\gamma X$

The following partonic subprocesses contribute to the process $ep \longrightarrow \nu\gamma X$:

$$eu \longrightarrow \nu\gamma d,$$

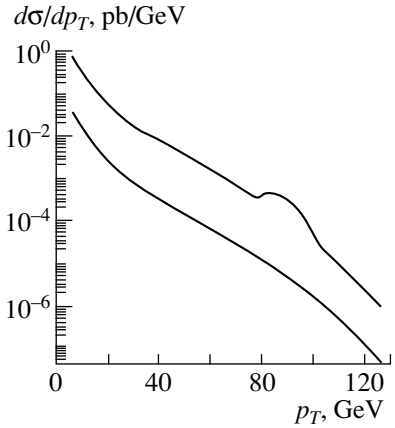

Fig. 4. The $ep \longrightarrow \nu\gamma X$ cross section as a function of the photon transverse momentum in the SM case.

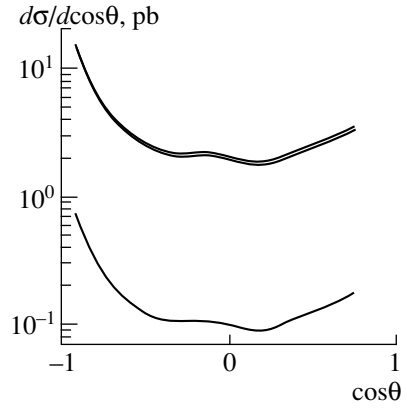

Fig. 5. Angular dependence of the $ep \longrightarrow \nu\gamma X$ cross section in the SM case.

$$eu \longrightarrow \nu\gamma s,$$
$$eu \longrightarrow \nu\gamma b.$$

For each of the cases, the corresponding Feynman diagrams are shown in Fig. 1. Since the signal topology for this process includes a jet, a photon, and missing energy, it is necessary to require the jet–photon separation (for example, by applying the cut on the relative pseudorapidity of the photon and jet, $\Delta\eta$, and their relative azimuthal angle, $\Delta\varphi$) and to impose the cut on the photon transverse momentum to get rid of the collinear and infrared singularities.

This process was studied in detail in the literature [1]; however, we will recall some of its main features to motivate our further choice of kinematical cuts that are aimed at improving the sensitivity of the process to anomalous couplings. We found that the cuts

$$p_T^\gamma \geq 0.5 \text{ GeV and } \sqrt{(\Delta\eta)^2 + (\Delta\varphi)^2} \geq 0.4 \qquad (4)$$

allow one to isolate the singularities and to separate the final photon and the jet. With these cuts, the cross sections for the relevant subprocess are

$$\sigma(eu \longrightarrow \nu\gamma d) = 8.72 \text{ pb},$$
$$\sigma(eu \longrightarrow \nu\gamma s) = 0.44 \text{ pb},$$
$$\sigma(eu \longrightarrow \nu\gamma b) = 1.06 \times 10^{-4} \text{ pb},$$

which corresponds to the $ep \longrightarrow \nu\gamma X$ total cross section of $\simeq 9.16$ pb. The contribution from the subprocess with a b quark in the final state is negligible, and we will not show it, while presenting differential distributions, but will keep it performing numerical estimates.

The differential distributions with respect to the photon transverse momentum, its scattering angle (relative to the electron-beam direction), and energy are shown in Figs. 4–6. In all three figures, the lowest curve represents the contribution from the subprocess with an s quark in the final state, while intermediate and upper curves represent, respectively, the contribution of the final d quark and the total contribution (in the cases of p_T and E distributions, the last two curves are indistinguishable on this scale). One can see that the bulk of the cross section is collected at low values of the photon transverse momentum and energy.

It is seen from the diagrams in Fig. 1 that the anomalous terms contribute to the process $ep \longrightarrow \nu\gamma X$ only through the $WW\gamma$ vertex. This means that, in terms of (3), the total cross section and the differential distributions that take into account anomalous interactions are functions of the combination $(L_{9L} + L_{9R})$ of anomalous couplings, which parametrize the $WW\gamma$ vertex. From Fig. 7, where the total cross section is shown as a function of $(L_{9L} + L_{9R})$, one can see that the total cross section has the highest sensitivity at negative values of $(L_{9L} + L_{9R})$; this is due to the constructive (destructive) interference between the anomalous and the Standard Model contributions at negative (positive) values of $(L_{9L} + L_{9R})$. Analyzing the process distributions, we found that stricter bounds on the anomalous couplings can be attained from the data on p_T distributions. Therefore, it seems interesting to study the behavior of $d\sigma/dp_T$ for nonvanishing anomalous couplings.

In Fig. 8, we present[3)] the relative contributions of the anomalous terms to the p_T distribution for $(L_{9L} + L_{9R}) = 500$ and -500[4)] (curves *1* and *2*, respectively). One can see that, for positive values of the anomalous couplings, the new-physics contribution is positive and corresponds to the high-p_T region, while, for negative values, it is distributed more or less uniformly over the region of moderate p_T. In either case, however, the region of small p_T is poorly sensitive to new-physics effects; i.e., it is mostly dominated by the SM contribution. This allows one to impose an extra cut on p_T, which should suppress the "background" SM contribution without losses of the effect due to anomalous terms. The optimal cut on p_T can be determined from

[3)]The appearance of sharp peaks in Figs. 8 and 9 is caused by a shortcoming in the spline algorithm.

[4)]These values of $(L_{9L} + L_{9R})$ were chosen for demonstration purposes only.

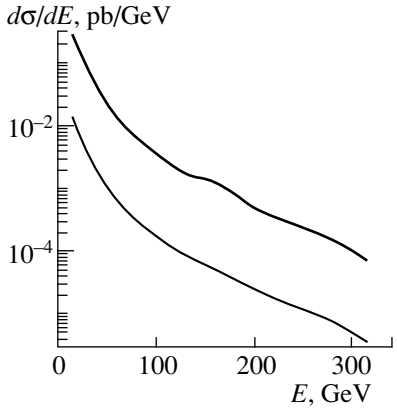

Fig. 6. Energy dependence of the $ep \longrightarrow \nu\gamma X$ cross section in the SM case.

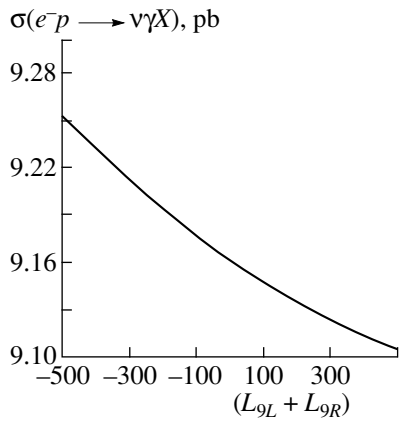

Fig. 7. $ep \longrightarrow \nu\gamma X$ total cross section as a function of anomalous couplings.

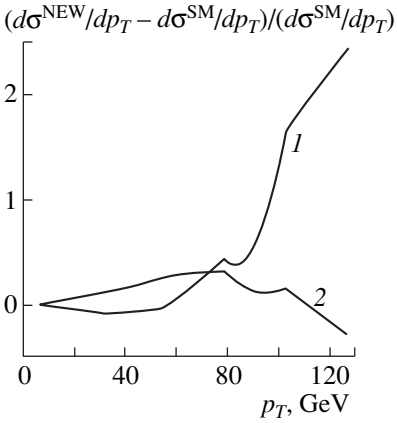

Fig. 8. Relative deviation of the p_T distribution for the process $ep \longrightarrow \nu\gamma X$ at nonvanishing anomalous couplings.

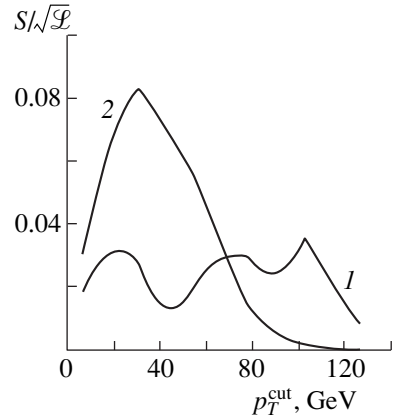

Fig. 9. Normalized sensitivity as a function of p_T^{cut}.

the so-called "sensitivity function," which is defined as

$$S = \frac{\left|\sigma^{\text{NEW}} - \sigma^{\text{SM}}\right|}{\sqrt{\sigma^{\text{SM}}}}\sqrt{\mathscr{L}}, \qquad (5)$$

where σ^{SM} and σ^{NEW} are the SM cross section and the cross section with allowance for the anomalous terms, respectively. The appearance of a peak in $S(p_T^{\text{cut}})$ corresponds to the optimal cut value. In Fig. 9, the sensitivity function is plotted against p_T^{cut} for the case of $(L_{9L} + L_{9R}) = 500$ and -500 (curves *1* and *2*, respectively). It should be noted that a variation of the couplings will change the absolute normalization of the curves, but this will not modify their line shape. One can see that, for negative coupling values, the sensitivity peaks are at $p_T^{\text{cut}} \simeq 30$ GeV, while for positive coupling values, there is no such pronounced peak behavior. Maximizing both *S* functions, one gets an optimal cut value, $p_T \geq 30$ GeV. Later, discussing the resulting bounds, we will use just this cut value. This cut does lead to a higher sensitivity of the cross section to anomalous couplings.

In Fig. 10, we again present the total cross section as a function of $(L_{9L} + L_{9R})$, but for the case where the cut $p_T \geq 30$ GeV is used. Of course, this cut reduces the cross section substantially; however, while, in the no-cut case (see Fig. 7), the cross section varies from 1 to –0.5%, for cut used, the cross section varies from 14 to –4.6% for the same range of $(L_{9L} + L_{9R})$ values.

3.2. Process $ep \longrightarrow eWX$

This process has a smaller cross section in relation to that for $ep \longrightarrow \nu\gamma X$, but it turns out to be very sensitive to the anomalous couplings. The following partonic subprocesses contribute to $ep \longrightarrow eWX$:

$$eu \longrightarrow eWd,$$
$$eu \longrightarrow eWs,$$
$$eu \longrightarrow eWb,$$
$$ed \longrightarrow eWu,$$
$$ed \longrightarrow eWc.$$

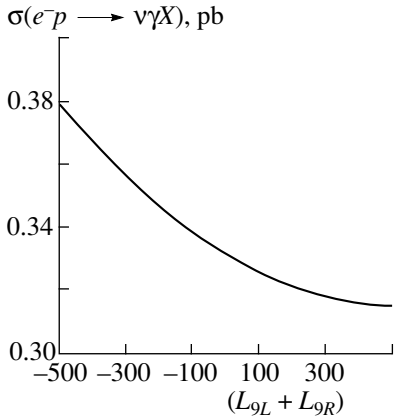

Fig. 10. $ep \longrightarrow \nu\gamma X$ total cross section as a function of anomalous couplings for $p_T \geq 30$ GeV.

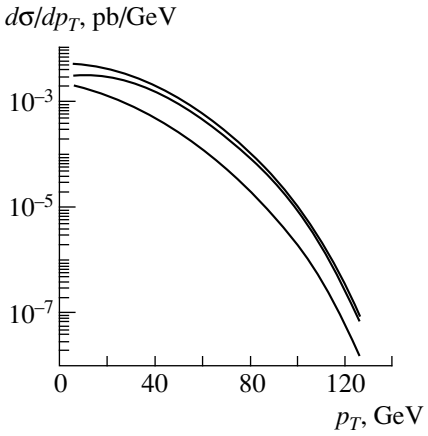

Fig. 11. $ep \longrightarrow eWX$ cross section versus the transverse momentum p_T of W in the SM case.

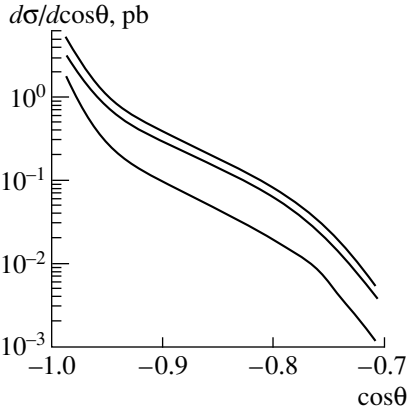

Fig. 12. $ep \longrightarrow eWX$ cross section versus the W scattering angle in the SM case.

The corresponding Feynman diagrams are shown in Fig. 2. For this process, the signal includes the scattered lepton, a jet, and final W-decay products. To regulate the singularities, it is necessary to impose a cut on the electron transverse momentum. This cut also solves, in part, the problem of the scattered electrons lost in the beam pipe. However, a cross-check cut on the polar angle of the scattered electrons is also needed, $-0.999 \leq \cos\theta_e \leq 0.998$, where θ_e is the angle of the scattered electron with respect to the electron-beam direction. It is also necessary to require the jet–electron separation, which could be done, for example, by applying the cut on the relative pseudorapidity of the electron and the jet and their azimuthal angle. In this case, we should identify final W by its decays into $l\nu$ or jets. The possible backgrounds to the leptonic W-decay mode are beam-induced processes, cosmic muons, charged-current events with a spurious electron, and the neutral-current background. As was shown in [6], these backgrounds can be reduced by imposing cuts on the position of the interaction vertex, by means of algorithms based on calorimeter and tracking information, by requiring an isolated electromagnetic cluster and a matched track, and by requiring an isolated missing p_T. It was found [6] that such cuts reduce the signal-to-background ratio up to 1/7 and lead to an acceptance of about 40–65% for $W \longrightarrow e\nu(\mu\nu, \tau\nu)$ events. For the hadronic decay modes of W, the dominant backgrounds are QCD processes from neutral-current DIS and photoproduction. Jet cuts and algorithms [6] being applied lead to a significant reduction of the background and give the signal-to-background ratio of 1/24.

To demonstrate the characteristic behavior of the $ep \longrightarrow eWX$ process distributions, we use a minimal set of cuts, $p_T^e \geq 2$ GeV and the cut on the electron-scattering angle discussed above. In this case, the subprocess cross sections are

$$\sigma(eu \longrightarrow eWd) = 1.39 \times 10^{-1} \text{ pb},$$
$$\sigma(eu \longrightarrow eWs) = 0.738 \times 10^{-2} \text{ pb},$$
$$\sigma(eu \longrightarrow eWb) = 1.694 \times 10^{-6} \text{ pb},$$
$$\sigma(ed \longrightarrow eWu) = 0.617 \times 10^{-1} \text{ pb},$$
$$\sigma(ed \longrightarrow eWc) = 0.32 \times 10^{-2} \text{ pb},$$

which corresponds to the total cross section for $ep \longrightarrow eWX$ of about 0.21 pb. In Figs. 11–14, we present the process differential distributions in the transverse momentum and scattering angle of W and the electron, respectively. In all these figures, the lowest curve represents the contribution from the d-quark subprocesses, while the intermediate and upper curves represent the u-quark and total contributions. Both the W-boson and electron p_T distributions are strongly peaked at small p_T. While produced W bosons are boosted along the proton direction, the angular distribution for electrons is not so sharp and they are scattered preferably along the electron-beam direction.

Anomalous couplings contribute to the process $ep \longrightarrow eWX$ through the WWZ and $WW\gamma$ vertices, and this implies that it is possible in principle to separate L_{9L} and L_{9R} dependences in the observables. The pro-

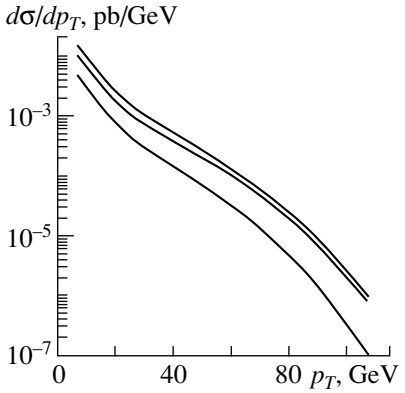

Fig. 13. $ep \longrightarrow eWX$ cross section versus the transverse momentum p_T of the electron in the SM case.

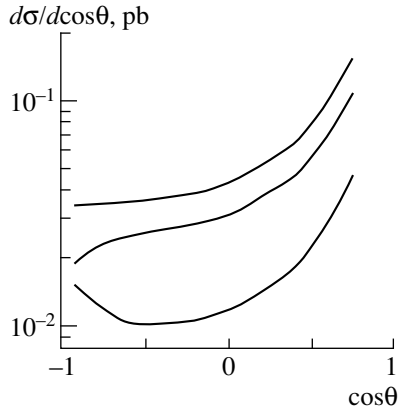

Fig. 14. $ep \longrightarrow eWX$ cross section versus the electron-scattering angle in the SM case.

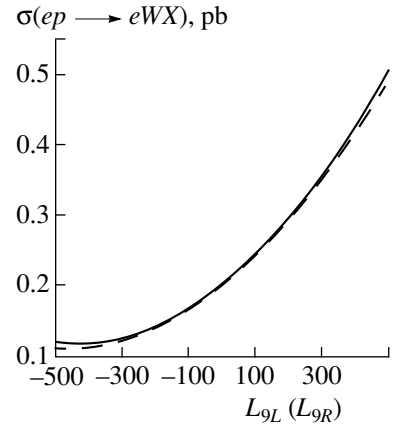

Fig. 15. $ep \longrightarrow eWX$ total cross section as a function of the couplings L_{9L} and L_{9R}.

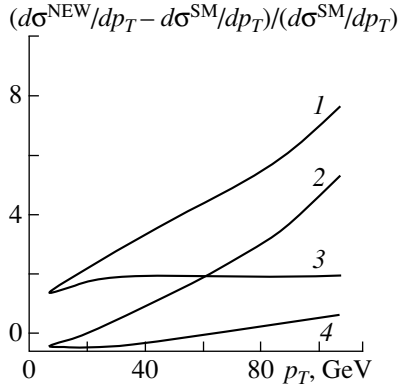

Fig. 16. Relative deviation of the electron p_T distribution for the $ep \longrightarrow eWX$ process at nonvanishing anomalous couplings.

cess cross section reveals a sensitivity to both couplings [see Fig. 15, which shows the total cross section as a function of the couplings L_{9L} (solid curve) and L_{9R} (dashed curve)], much higher than that for the $ep \longrightarrow \nu\gamma X$ case. We analyzed various observables and found that the most severe bounds on the anomalous parameters can be obtained from the differential distribution over the electron transverse momentum. In Fig. 16, we demonstrate the relative deviation of this distribution for nonvanishing values of the couplings L_{9L} and L_{9R}, where curve *1* (*2*) corresponds to the case of L_{9L} = 500 (–500), L_{9R} = 0, and curve *3* (*4*) corresponds to $L_{9L} = 0, L_{9R} = 500$ (–500). One can see that, for negative couplings, the deviation is less than that for the case of positive couplings, and it is negative for low p_T^e, which is due to the destructive interference with SM contribution. For both cases, the anomalous-coupling contribution reaches its maximum in the high p_T^e region. We used the sensitivity function defined in (5) to determine the p_T^e cut that makes the process be sensitive to anomalous contributions; however, it turned out that, due to the small cross section and, as a consequence, low statistics, such a cut does not lead to noticeable improvement of the resulting bounds.

3.3. Process $ep \longrightarrow \nu WX$

The last process to be considered is $ep \longrightarrow \nu WX$. The partonic subprocesses contributing to $ep \longrightarrow eWX$ are as follows:

$$eu \longrightarrow \nu Wc,$$
$$eu \longrightarrow \nu Wu,$$
$$ed \longrightarrow \nu Wd,$$
$$ed \longrightarrow \nu Ws,$$
$$ed \longrightarrow \nu Wb.$$

The corresponding Feynman diagrams are shown in Fig. 3. For this process, the signal includes the missing p_T, a jet, and final W-decay products. The cut $p_T \geq 5$ GeV on the transverse momentum of the struck quark jet allows one to get rid of singularities and to guarantee a

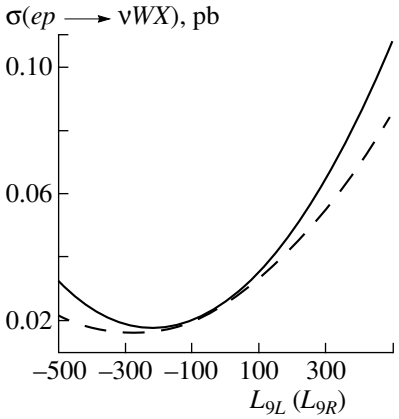

Fig. 17. $ep \longrightarrow \nu WX$ total cross section as a function of anomalous couplings.

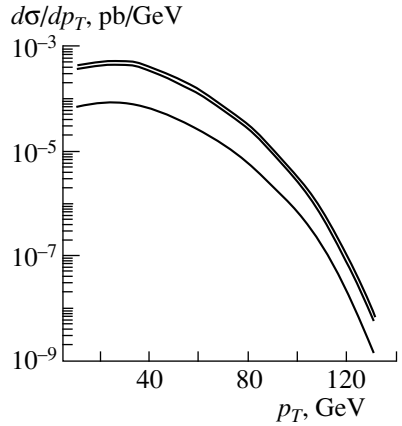

Fig. 18. $ep \longrightarrow \nu WX$ cross section versus the W transverse momentum.

high detection efficiency. As in the case of the process $ep \longrightarrow eWX$, one has to reconstruct the final W boson by its leptonic or jet final states. In doing this, all the methods and cuts necessary to reconstruct the final state and to suppress the background discussed in the preceding section are also applicable.

For the cut on the jet transverse momentum, $p_T \geq 5$ GeV, the partial cross sections the various partonic subprocesses are

$$\sigma(eu \longrightarrow \nu Wu) = 2.11 \times 10^{-2} \text{ pb},$$

$$\sigma(ed \longrightarrow \nu Wd) = 0.41 \times 10^{-2} \text{ pb},$$

and the subprocesses with a s, c, or b quark in the final state have cross sections that are negligibly small. The total cross section is about 2.5×10^{-2} pb, which is much smaller than that for the processes $ep \longrightarrow \nu\gamma X$ or $ep \longrightarrow eWX$. For an integrated luminosity of 1000 pb^{-1} and a realistic reconstruction efficiency, one could expect to have only isolated signal events, at max. However, this reaction is highly sensitive to an anomalous contribution.

In Fig. 17, which shows the total cross section as a function of anomalous couplings, one can see that the process cross section is highly sensitive to positive values of anomalous couplings. In Figs. 18 and 19, we present the distributions of the cross section with respect to the transverse momentum and W scattering angle. One can see that the bulk of the cross section is collected from the small p_T region and that final W bosons are strongly boosted along the proton-beam direction. Though both distributions are equally sensitive to an anomalous contribution, the fact that the process cross section is extremely small makes it reasonable to analyze the total cross section only, since the low statistics will hardly allow observation of the real distributions for this process.

4. BOUNDS ON ANOMALOUS COUPLINGS

In this section, we will discuss the bounds on the anomalous couplings that can be attained from the data on the processes $ep \longrightarrow \nu\gamma X$ (eWX, νWX). First of all, it is necessary to determine the efficiencies of the final-state reconstruction for each of the processes.

For the reaction $ep \longrightarrow \nu\gamma X$, which has a final-state topology of a jet and a photon plus missing energy, it should be noted that existing calorimeters allow one to detect energetic photons with the efficiency of about 60%. However, about 30% of all photons convert to electron–positron pairs on the detector material before entering the calorimeter. The reconstruction efficiency of such pairs is about 90%. Thus, the expected reconstruction efficiency for the photon is about 70%. Putting bounds on the anomalous couplings from this process, we use the cut set of (4), but with $p_T \geq 30$ GeV, as follows from the sensitivity-function analysis.

Studying the process $ep \longrightarrow eWX$, we adopt the algorithms and cuts used in [6], thus having the following acceptances for each of W-decay modes: 65% for $W \longrightarrow e\nu(\mu\nu)$, 40% for $W \longrightarrow \tau\nu$, and 20% for $W \longrightarrow$ jets. In addition, we check the cuts $p_T^e \geq 5$ GeV and $-0.999 \leq \cos\theta_e \leq 0.998$ to be satisfied, which ensures the scattered-electron detection.

For the process $ep \longrightarrow \nu WX$, we require $p_T \geq 5$ GeV for the struck quark and adopt the corresponding algorithms for reconstructing final W decay as discussed above.

For an integrated luminosity of 1000 pb^{-1}, we assume the uncertainty in the luminosity to be 2% and the systematics to be 1% for each of the acceptances.

Discussing the sensitivity of the processes to anomalous couplings, we will analyze the differential cross sections in the case of $ep \longrightarrow \nu\gamma X$ and $ep \longrightarrow eWX$ and the total cross section in the case of $ep \longrightarrow \nu WX$ (here, under the assumption of the Gaussian nature of the systematics, one can relate the deviations of σ_{tot} to the cor-

responding confidence level). We adopt the following philosophy to confine anomalous contributions: one uses the SM predictions as "experimental" data and considers possible effects due to new physics as small deviations. One then requires agreement between the predictions including new physics and the "experimental" values within expected experimental errors. Thus, the parameters representing new physics are bound by requiring that their effect on the observables not exceed the expected experimental errors.

Using differential cross sections (p_T or angular distributions), we apply the simplest χ^2 criterion defined as

$$\chi^2 = \sum_i \left(\frac{X_i - Y_i}{\Delta^i_{\text{exp}}} \right)^2, \qquad (6)$$

where, for example, for the case of the p_T distribution,

$$X_i = \int_{p_T^i}^{p_T^{i+1}} \frac{d\sigma^{\text{SM}}}{dp_T} dp_T, \quad Y_i = \int_{p_T^i}^{p_T^{i+1}} \frac{d\sigma^{\text{NEW}}}{dp_T} dp_T.$$

In the above expressions, $\sigma \equiv \sigma^{\text{SM}}$ represents the experimental data, σ^{NEW} are the new-model predictions, and Δ^i_{exp} are the appropriate experimental errors in bins including statistical and systematic errors. For binning, we subdivide the chosen kinematical range into equal bins. Here,

$$\Delta^i_{\text{exp}} = X_i \sqrt{\delta^2_{\text{stat}} + \delta^2_{\text{syst}}}.$$

In Fig. 20, we present the resulting allowed regions (for a 95% C.L. and $\Lambda = 2$ TeV) for the parameters L_{9L} and L_{9R} that can be attained from the data on the process $ep \longrightarrow \nu\gamma X$ (the area bounded by long-dashed lines), $ep \longrightarrow eWX$ (the domain bounded by the solid contour), and $ep \longrightarrow \nu WX$ (the area bounded by the short-dashed contour). One can see that, in the case of $ep \longrightarrow \nu\gamma X$, the resulting bounds on L_{9L} and L_{9R} have the form of a straight band oriented along the line $L_{9L} = -L_{9R}$. This is due to the fact that these couplings contribute to the process $ep \longrightarrow \nu\gamma X$ only through the parameter κ_γ of the anomalous $WW\gamma$ vertex, and κ_γ is proportional to the combination $(L_{9L} + L_{9R})$ [see (3)]. However, due to the different sensitivity of the data to the regions of negative and positive coupling values, this band is not symmetric with respect the line $L_{9L} = -L_{9R}$. In two other processes anomalous parameters contribute through both the $WW\gamma$ and the WWZ vertices; thus, the resulting bounds are less trivial.

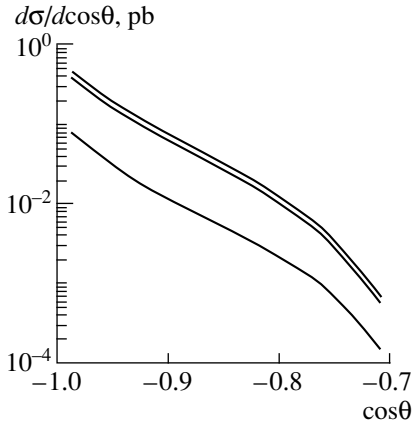

Fig. 19. $ep \longrightarrow \nu WX$ cross section versus the cosine of the W scattering angle.

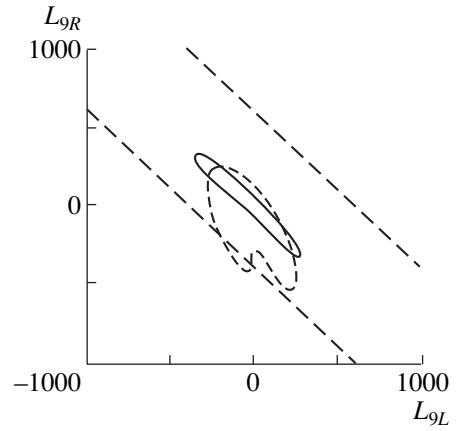

Fig. 20. Allowed region (at a 95% C.L.) for the couplings L_{9L} and L_{9R} from the data on $ep \longrightarrow \nu\gamma X$ (the area between long-dashed lines), $ep \longrightarrow eWX$ (domain within the solid contour), and $ep \longrightarrow \nu WX$ (domain within the short-dashed contour).

Thus, for $\mathcal{L} = 1000$ pb^{-1}, $\Lambda = 2$ TeV, and a 95% C.L., one gets the following two-parameter bounds from the individual processes:

Process	Bounds
$ep \longrightarrow \nu\gamma X$	$-390 \le L_{9L} + L_{9R} \le 600$
$ep \longrightarrow eWX$	$-340 \le L_{9L} \le 280$
	$-330 \le L_{9R} \le 320$
$ep \longrightarrow \nu WX$	$-280 \le L_{9L} \le 260$
	$-530 \le L_{9R} \le 260$

One can see that, with the two-parameter fit, the bounds coming from the last two processes are narrower than those from $ep \longrightarrow \nu\gamma X$. It is important that the bounds resulting from the $ep \longrightarrow \nu WX$ data, in spite of the small cross section for the process, are quite stringent and turn out to be complementary to those

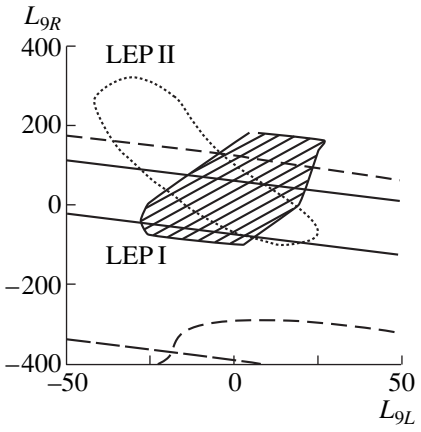

Fig. 21. Allowed regions (at a 95% C.L.) for couplings L_{9L} and L_{9R} from LEP I (shaded domain) [12], LEP II (domain within the dotted contour) [15], and HERA processes (the notation for curves is identical to that in Fig. 20).

from the process $ep \longrightarrow eWX$. In the case of a one-parameter fit, i.e., when only one coupling is varied at a time, the individual bounds from the last two processes become narrower:

Process	Bounds
$ep \longrightarrow eWX$	$-75 \le L_{9L} \le 55$
	$-80 \le L_{9R} \le 60$
$ep \longrightarrow \nu WX$	$-250 \le L_{9L} \le 100$
	$-290 \le L_{9R} \le 120$

Of course, it is interesting to compare these bounds with those coming from the processes at LEP I and LEP II. It was shown [12] that accurate measurements of Z partial widths imply

$$-28 \le L_{9L} \le 27,$$
$$-100 \le L_{9R} \le 190.$$

The expected bounds [15] from LEP II coming from data on the process $e^+e^- \longrightarrow W^+W^-$ at $\sqrt{s}$ = 190 GeV and an integrated luminosity of 500 pb^{-1} are

$$-41 \le L_{9L} \le 26,$$
$$-100 \le L_{9R} \le 330.$$

In Fig. 21, we present the 95% C.L. bounds on the couplings L_{9L} and L_{9R} that follow from the analysis of Z partial widths (shaded domain), data on the process $e^+e^- \longrightarrow W^+W^-$ at LEP II (dotted contour), and data on HERA processes (the notation for bounding contours is identical to that in Fig. 20).

One can see that the bounds from $ep \longrightarrow \nu\gamma X$ are more flexible than LEP I or LEP II results. However, both the process $ep \longrightarrow eWX$ and the process $ep \longrightarrow \nu WX$ provide bounds that can be considered as complementary to the LEP I and LEP II results. It turns out that the data on the HERA processes are unable to improve the bounds on the coupling L_{9L}, but they reduce significantly the allowed region for L_{9R}. A combined analysis of the data from LEP I, LEP II, and HERA could exclude a large portion of the allowed domain for the couplings in the region of large positive L_{9R} values and slightly improve the LEP I + LEP II bounds for negative L_{9R} values.

5. CONCLUSION

We have presented a comparative analysis of the $ep \longrightarrow \nu\gamma X$ (eWX, νWX) process sensitivity to anomalous couplings that parametrize the $WW\gamma(Z)$ vertices. For anomalous couplings, we used the approach of the effective Lagrangian and considered the model where the electroweak-symmetry sector is strongly coupled and there is no light Higgs particles. We found that the processes $ep \longrightarrow \nu\gamma X$ (eWX, νWX) reveal a high sensitivity to anomalous contributions. In spite of the small cross section, the processes $ep \longrightarrow eWX$ (νWX) provide the most severe bounds on the anomalous parameters.

At the HERA collider with an integrated luminosity of 1000 pb^{-1}, one can confine the anomalous couplings with a 95% C.L. at the level of

$$-390\left(\frac{\Lambda}{2\ \text{TeV}}\right)^2 \le L_{9L} + L_{9R} \le 600\left(\frac{\Lambda}{2\ \text{TeV}}\right)^2$$

from the data on the process $ep \longrightarrow \nu\gamma X$;

$$-75\left(\frac{\Lambda}{2\ \text{TeV}}\right)^2 \le L_{9L} \le 55\left(\frac{\Lambda}{2\ \text{TeV}}\right)^2,$$

$$-80\left(\frac{\Lambda}{2\ \text{TeV}}\right)^2 \le L_{9R} \le 60\left(\frac{\Lambda}{2\ \text{TeV}}\right)^2$$

from the $ep \longrightarrow eWX$ data; and

$$-250\left(\frac{\Lambda}{2\ \text{TeV}}\right)^2 \le L_{9L} \le 100\left(\frac{\Lambda}{2\ \text{TeV}}\right)^2,$$

$$-290\left(\frac{\Lambda}{2\ \text{TeV}}\right)^2 \le L_{9R} \le 120\left(\frac{\Lambda}{2\ \text{TeV}}\right)^2$$

from the $ep \longrightarrow \nu WX$ data. The bounds from the last two processes turn out to be complementary.

We conclude that, from the data on HERA processes, one is unable to improve the bounds on the coupling L_{9L} coming from LEP I and LEP II, but these data could result in significantly narrowing the allowed region for L_{9R}.

ACKNOWLEDGMENTS

The authors would like to express their gratitude to Prof. A. Wagner and members of the DESY Theory Group for kind hospitality during the visit to DESY,

where a part of this work was done. The authors would like to thank Prof. F. Schrempp for reading this manuscript and making valuable remarks and Dr. L. Gladilin for useful discussions on the data analysis.

This work was supported in part by the Russian Foundation for Basic Research (project nos. 99-02-16558 and 96215-96575) and INTAS-RFBR (grant no. 95I1300).

REFERENCES

1. T. Hilbig and H.Spiesberger, in *Proceedings 1991 Workshop on Physics at HERA*, Ed. by W. Buchmuller and G. Ingelman (DESY, Hamburg, 1992), Vol. 2, p. 973; Nucl. Phys. B **373**, 73 (1992); U. Baur and M. A. Doncheski, Phys. Rev. D **46**, 1959 (1992).
2. U. Baur and D. Zeppenfeld, Nucl. Phys. B **325**, 253 (1989).
3. U. Baur, J. A. M. Vermaseren, and D. Zeppenfeld, Nucl. Phys. B **375**, 3 (1992).
4. M. Bohm and A. Rosado, Z. Phys. C **42**, 479 (1989).
5. C. S. Kim, J. Lee, and H. S. Song, Z. Phys. C **63**, 673 (1994).
6. V. A. Noyes, in *Proceedings of 1995/1996 Workshop on Future Physics at HERA*, Ed. by G. Ingelman *et al.* (DESY, Hamburg 1996), Vol. 1, p. 190.
7. T. Appelquist and C. Bernard, Phys. Rev. D **22**, 200 (1980); A. Lunghitano, Nucl. Phys. B **188**, 118 (1981).
8. B. Holdom, Phys. Lett. B **258**, 156 (1991); A. Falk, M. Luke, and E. Simmons, Nucl. Phys. B **365**, 523 (1991); J. Bagger, S. Dawson, and G. Valencia, Nucl. Phys. B **399**, 364 (1993); T. Appelquist and G.-H. Wu, Phys. Rev. D **48**, 3235 (1993).
9. A. A. Likhoded, T. Han, and G. Valencia, Phys. Rev. D **53**, 4811 (1996).
10. S. Dawson, A. A. Likhoded, and G. Valencia, in *Proceedings of 1996 DPF/DPB Summer Study on New Directions for High-Energy Physics (Snowmass 96)*; hep-ph/9610299.
11. K. Hagiwara *et al.*, Nucl. Phys. B **282**, 253 (1987).
12. S. Dawson and G. Valencia, Nucl. Phys. B **439**, 3 (1995); Phys. Lett. B **333**, 207 (1994).
13. CTEQ Collab. (H. L. Lai *et al.*), Phys. Rev. D **55**, 1280 (1997).
14. Particle Data Group, Eur. Phys. J. C **3**, 1 (1998).
15. F. Boudjema, in *Proceedings of Workshop on Physics and Experiments with Linear e^+e^- Colliders*, Ed. by F. A. Harris *et al.* (World Sci., Singapore, 1993), p. 713 and references therein.